



SCUOLA INTERNAZIONALE SUPERIORE DI STUDI AVANZATI

SISSA Digital Library

Graphene oxide flakes tune excitatory neurotransmission in vivo by targeting hippocampal synapses

*Original*

Graphene oxide flakes tune excitatory neurotransmission in vivo by targeting hippocampal synapses / Rauti, Rossana; Medelin, Manuela; Newman, Leon; Vranic, Sandra; Reina, Giacomo; Bianco, Alberto; Prato, Maurizio; Kostarelos, Kostas; Ballerini, Laura. - In: NANO LETTERS. - ISSN 1530-6984. - 19:5(2019), pp. 2858-2870. [[10.1021/acs.nanolett.8b04903](https://doi.org/10.1021/acs.nanolett.8b04903)]

*Availability:*

This version is available at: 20.500.11767/89920 since: 2019-04-19T12:51:40Z

*Publisher:*

*Published*

DOI:[10.1021/acs.nanolett.8b04903](https://doi.org/10.1021/acs.nanolett.8b04903)

*Terms of use:*

Testo definito dall'ateneo relativo alle clausole di concessione d'uso

*Publisher copyright*

ACS - American Chemical Society

This version is available for education and non-commercial purposes.

note finali coverpage

(Article begins on next page)

1                   **Graphene Oxide Flakes Tune Excitatory**  
2                   **Neurotransmission In Vivo by Targeting Hippocampal**  
3                   **Synapses**

4    Rossana Rauti<sup>†</sup>, Manuela Medelin<sup>†,\*</sup>, Leon Newman<sup>‡</sup>, Sandra Vranic<sup>‡</sup>, Giacomo Reina<sup>§</sup>, Alberto  
5    Bianco<sup>§</sup>, Maurizio Prato<sup>‡,¶,Δ</sup>, Kostas Kostarelos<sup>‡#</sup>, Laura Ballerini<sup>†#</sup>

6    <sup>†</sup>Neuron Physiology and Technology Lab, International School for Advanced Studies (SISSA),  
7    Neuroscience, Trieste, Italy

8    <sup>\*</sup>Life Science Department, University of Trieste, Italy

9    <sup>‡</sup>Nanomedicine Lab, Faculty of Biology, Medicine & Health and National Graphene Institute, AV  
10   Hill Building, University of Manchester, Manchester, United Kingdom

11   <sup>§</sup>University of Strasbourg, CNRS, Immunology, Immunopathology and Therapeutic Chemistry,  
12   UPR 3572, 67000 Strasbourg, France

13   <sup>‡</sup>Department of Chemical and Pharmaceutical Sciences, University of Trieste, Trieste, Italy

14   <sup>¶</sup>Nanobiotechnology Laboratory, CIC biomaGUNE, San Sebastián, Spain

15   <sup>Δ</sup>Ikerbasque, Basque Foundation for Science, Bilbao, Spain

16   KEYWORDS: graphene, synapses, hippocampal network, glutamate, quantum dots.

17

18

## 19 ABSTRACT

20 Synapses compute and transmit information to connect neural circuits and are at the basis of brain  
21 operations. Alterations in their function contribute to a vast range of neuropsychiatric and  
22 neurodegenerative disorders and synapse-based therapeutic intervention, such as selective  
23 inhibition of synaptic transmission, may significantly help against serious pathologies. Graphene  
24 is a two-dimensional nanomaterial largely exploited in multiple domains of science and  
25 technology, including biomedical applications. In hippocampal neurons in culture, small graphene  
26 oxide nanosheets (s-GO) selectively depress glutamatergic activity without altering cell viability.  
27 Glutamate is the main excitatory neurotransmitter in the central nervous system and growing  
28 evidence suggests its involvement in neuropsychiatric disorders. Here we demonstrate that s-GO  
29 directly targets the release of pre-synaptic vesicle. We propose that s-GO flakes reduce the  
30 availability of transmitter, via promoting its fast release and subsequent depletion, leading to a  
31 decline of glutamatergic neurotransmission. We injected s-GO in the hippocampus in vivo, and  
32 forty-eight hours after surgery ex vivo patch-clamp recordings from brain slices show a significant  
33 reduction in glutamatergic synaptic activity, in respect to saline injections.

34

35

36

37

38

39 Graphene is a 2D material made of  $sp^2$ -hybridized carbon atoms organized in a hexagonal lattice  
40 and characterized by excellent physical features, including outstanding electron mobility and  
41 mechanical flexibility.<sup>1-3</sup> Because of its properties,<sup>4-6</sup> graphene is considered a rising star in a  
42 growing number of technological developments, including biomedical ones.<sup>2,4,5,7</sup> In neurology,  
43 graphene-based neuronal implants or bio-devices, may overcome current technical limitations in  
44 treating pathologies that range from neurooncology to neuroregeneration.<sup>8,9</sup> We reported recently  
45 the ability of small, thin graphene oxide sheets (s-GO) to alter specifically neuronal synapses, with  
46 no impact on cell viability. In particular, in cultured hippocampal networks, upon chronic long-  
47 term exposure to s-GO, glutamatergic release sites were sized down.<sup>10</sup> It is well known that  
48 glutamate is the main excitatory neurotransmitter in the mammalian central nervous system (CNS)  
49 and mediates neuronal development, migration, synaptic maintenance and transmission.<sup>11-13</sup> An  
50 uncontrolled release of glutamate in the extracellular space may lead to excitotoxicity,  
51 neurodegeneration and neurological disorders, including pain.<sup>14</sup> Localized targeting and fine-  
52 tuning of the glutamatergic system are attractive objectives in neuroscience. To achieve a deep  
53 understanding of the interactions between s-GO and the machinery governing nerve cell functions  
54 is mandatory to translate these findings into potential therapeutic applications. In particular,  
55 graphene translocation or adhesion to cell membranes<sup>15,16</sup> may potentially interfere with activities  
56 such as the exocytic and endocytic trafficking systems, essential to physiological synaptic  
57 transmission.<sup>15,17</sup> Here, we describe, by single cell electrophysiology, how s-GO nanosheets  
58 acutely tune synaptic release in excitatory synapses of hippocampal cultured neurons and acute  
59 slices, by interfering with the probability of vesicle release. We propose that such interference  
60 leads to transmitter depletion and subsequent depression of the glutamatergic activity. We next  
61 address whether such material similarly affects glutamatergic transmission in vivo, by injecting s-

62 GO in the dentate gyrus of the hippocampus of juvenile rats. We patch-clamped single neurons  
63 from ex vivo hippocampal slices, 48 h and 72 h after s-GO microinjections. We demonstrate that  
64 s-GO targets and down-regulates glutamatergic synapses in vivo and further illustrates the  
65 potential of s-GO flakes to be engineered as specific synaptic transmission modulators.

66 **GO functionalization and characterization.** The produced s-GO dispersion was visually  
67 homogenous and of a brownish-translucent appearance. The dispersions did not show any evidence  
68 of sedimentation or any other observable changes for over 6 months, indicating their physical  
69 stability. The characterization of the s-GO nanosheets is presented in Figure 1 and in  
70 Supplementary Figure S1. The morphological features of the s-GO nanosheets were examined  
71 using AFM (Figure 1a) and TEM (Supplementary Figure S1a). Both analytical methods showed  
72 that the lateral dimension of the s-GO nanosheets was predominantly between 100–300 nm with  
73 very few larger sheets into the  $\mu\text{m}$  range (Figure 1b). Moreover, AFM revealed that the material is  
74 composed of sheets from single to few-layer thickness (Supplementary Figure S1b). The material  
75 structural features were studied by Raman spectroscopy which evidenced the presence of the  
76 characteristic G and D scatter bands at  $1595\text{ cm}^{-1}$  and  $1330\text{ cm}^{-1}$ , respectively (Figure 1c). The D  
77 scatter band was markedly higher than the G band. The intensity ratio of these two peaks, known  
78 as the  $I(\text{D})/I(\text{G})$ , was calculated to be  $1.31 \pm 0.01$ , indicating that the material hexagonal lattice  
79 was defected. XPS analysis corroborated to the presence of functional groups (Supplementary  
80 Figure S1c) and further indicated that the defects correspond to oxygen-containing functionalities.  
81 The C/O ratio was found to be 2.1 and the material chemical purity was 99.8 %.<sup>18</sup> The surface  
82 functionalization was further supported by laser Doppler electrophoresis to indicate that the  
83 dispersed sheets had a surface charge of  $-55.9 \pm 1.4\text{ mV}$ . Aiming to track the s-GO flakes within  
84 neuronal tissue we performed covalent labeling of s-GO with quantum dot (QD) luminescent

85 nanoparticles. For this purpose, we first synthesized the AgInS<sub>2</sub>/ZnS-doped QDs capped with  
86 cysteine as described in the literature (see TEM images in Supplementary Figure S1d).<sup>19,20</sup>  
87 Subsequently, the coupling with s-GO was achieved via epoxy ring opening with the amino groups  
88 of the cysteine-capping agent. TEM microscopy shows the presence of small dark dots on the s-  
89 GO sheets associated with the presence of QDs on the surface (Supplementary Figure S1e,  
90 indicated by the arrows) as confirmed by XPS survey analysis (Figure 1d). The UV-Vis spectrum  
91 (Figure 1e) of the functionalized material showed a broadening of the absorption band between  
92 300 and 600 nm due to the presence of the nanocrystals onto GO. Fluorescence characterization is  
93 reported in Figure 1f; s-GO showed an emission centered at 585 nm attributed to the electronic  
94 transitions from the bottom of conductive band and the nearby localized states to the valence  
95 band.<sup>21</sup> QDs have an emission centered at 706 nm due to transition between the conductive band  
96 and the defected carbon lattice.<sup>22</sup> Interestingly, when QD were coupled to graphene oxide only s-  
97 GO luminescence was detected. The quenching of the QD emission may be attributed to an  
98 interfacial electron transfer between the QDs and the s-GO surface due to their close proximity.<sup>23,24</sup>  
99 Surprisingly, the emission band centered at 585 nm, attributed to the GO photoluminescence,  
100 appeared stronger in the case of QD-s-GO than in non-modified s-GO. Most probably, the energy  
101 transfer process causes the decrease of donor emission (QD quenching) and increase the s-GO  
102 acceptor emission<sup>24</sup> allowing us to visualize the s-GO-QD in the biological environment (vide  
103 infra).

104 **s-GO targets synaptic vesicle release at glutamatergic synapses in cultured hippocampal**  
105 **neurons.** To unravel the mechanisms by which thin s-GO sheets affect neurotransmission, we  
106 patch-clamped cultured hippocampal neurons while a second pipette for the local delivery of  
107 standard saline solution of s-GO (100 µg/mL; see Methods) was positioned at 200 µm distance (by

108 microscopic guidance) from the recorded neuron (sketched in Figure 2a). We estimated that, at  
109 this distance, the application of a brief (500 ms) pulse of pressure should result in a local (i.e. on  
110 the patched cell) and transient delivery of s-GO at a concentration of at least 10 % of that contained  
111 in the pipette (see Methods). Spontaneous synaptic activity was recorded in the presence of  
112 Tetrodotoxin, (TTX; 1  $\mu$ M). In TTX, synaptic events, termed miniature post synaptic currents  
113 (mPSCs), reflect the pre-synaptic, stochastic release of vesicles at individual synaptic terminals  
114 impinging on the recorded neuron. mPSCs frequency reflects the pre-synaptic release probability  
115 and on the number of synaptic contacts, while mPSCs amplitude is dictated by postsynaptic  
116 receptor sensitivity.<sup>25</sup> Baseline mPSCs were sampled before and after the local ejection of saline  
117 or s-GO (Figure 2b). In cultured neurons, virtually all mPSCs were made up by excitatory (AMPA  
118 glutamate receptor-mediated) events, identified by their fast kinetics (decay time constant  $\tau = 5 \pm$   
119  $0.5$  ms;<sup>26</sup>), and were thus named excitatory mPSCs (mEPSCs). Figure 2b shows representative  
120 control (top) and s-GO (bottom) current tracings prior and after saline or s-GO solution,  
121 respectively, were pressure ejected. In control neurons mEPSCs frequency did not change (from  
122  $0.06 \pm 0.03$  Hz to  $0.065 \pm 0.04$  Hz after saline-ejection,  $n = 14$ ; bar plot in Figure 2c, left). On the  
123 contrary, acute s-GO ejection significantly increased (\*  $P < 0.05$  Student's t-test) the mEPSCs  
124 frequency (from  $0.04 \pm 0.01$  Hz to  $0.12 \pm 0.02$ ,  $n = 13$ ; bar plot in Figure 2c, left). The increase in  
125 mEPSCs appeared with 8-10 s delay from the local s-GO ejection and completely reversed to  
126 baseline values ( $0.04 \pm 0.01$  Hz) 8-9 min following the acute application (bar plot in Figure 2c,  
127 left). In all treatments, the mEPSCs amplitude was not affected (bar plot in Figure 2c, right). These  
128 transient changes in the frequency of mEPSCs suggest a direct interference of s-GO with the  
129 presynaptic release machinery<sup>27,28</sup> and are consistent with the hypothesized targeting by s-GOs of  
130 endo-exocytotic mechanisms. This hypothesis is also validated by the co-localization of bassoon

131 (pre-synaptic terminal marker<sup>29</sup>) and s-GO detected by confocal microscopy in a different set of  
132 experiments, where s-GO was incubated (20  $\mu\text{g}/\text{mL}$ ; 30 min), before fixation of the cultures (see  
133 Methods; Supplementary Figure S2 a and b, controls and s-GO, respectively). We further address  
134 the dependency of these effects on the flakes' size. We adopted the same protocol to press-eject  
135 GO flakes (same concentration as s-GO) characterized by different lateral dimensions: large GO  
136 (l-GO,  $\approx 2 \mu\text{m}$ ) or ultra-small GO (us-GO,  $\approx 40 \text{ nm}$ ).<sup>18</sup> Supplementary Figure S2 c shows  
137 representative control (top) and l-GO (bottom) current tracings sampled before and after the local  
138 ejection of saline or l-GO solutions. Opposite to s-GO, l-GO did not change mEPSCs frequency  
139 (from  $0.06 \pm 0.01 \text{ Hz}$  to  $0.07 \pm 0.02 \text{ Hz}$  after saline ejection,  $n = 5$ ; from  $0.05 \pm 0.01 \text{ Hz}$  to  $0.07 \pm$   
140  $0.02 \text{ Hz}$  after l-GO ejection,  $n = 5$ ). Similarly (Supplementary Figure S2 d), us-GO did not  
141 modulate mEPSCs frequency (from  $0.05 \pm 0.01 \text{ Hz}$  to  $0.07 \pm 0.02 \text{ Hz}$ , after saline,  $n = 8$  and from  
142  $0.05 \pm 0.01 \text{ Hz}$  to  $0.07 \pm 0.02 \text{ Hz}$ , after us-GO,  $n = 8$ ).

143 Thus only s-GO transiently increased the frequency of mEPSCs. This apparent discrepancy with  
144 our previous results, where prolonged exposure to s-GO decreased glutamatergic activity,<sup>10</sup> may  
145 be explained by the emergence of glutamate depletion due to forced glutamate release. The latter  
146 leading to a transient facilitation followed, when s-GO is applied longer than the duration of the  
147 facilitatory effects, by a depression of vesicle release and thus a down-regulation of glutamate  
148 transmission.<sup>10</sup>

149 To investigate the s-GO interference with presynaptic release and whether this was truly selective  
150 for excitatory synapses, we tested the local delivery of s-GO nanosheets on the occurrence of  
151 evoked PSCs (ePSCs), by simultaneous whole-cell recordings from two monosynaptically  
152 connected neurons.<sup>26</sup> Action potentials were induced in the presynaptic neuron and the evoked  
153 postsynaptic unitary PSCs (delay 2 ms) were examined. In our in vitro system, monosynaptically

154 coupled pairs of neurons typically display either GABA<sub>A</sub> or glutamate AMPA receptor-mediated  
155 evoked currents.<sup>26,30,31</sup> We identified the different populations of ePSCs on the basis of their kinetic  
156 properties and pharmacology.<sup>26,32</sup> In fact, GABAergic ePSCs were characterized by a slow decay  
157 time constant ( $\tau = 23 \pm 7$  ms,  $n = 15$  for each condition, control and s-GO; Figure 2d, left) and  
158 were fully abolished by administration of 5  $\mu$ M Gabazine ( $n = 3$ ). Glutamatergic AMPA receptor–  
159 mediated ePSCs displayed fast decay ( $\tau = 7 \pm 1.2$  ms,  $n = 7$  for each condition; Figure 2d, right)  
160 and were further blocked by application of 10  $\mu$ M CNQX ( $n = 3$ ). To investigate the presynaptic  
161 properties we adopted paired-pulse stimulation protocols.<sup>33,34</sup> In paired-pulse stimulation the  
162 second response can be either facilitated or depressed. Usually, at a specific synapse, an increased  
163 probability of neurotransmitter release will favor paired-pulse depression, while a decrease in the  
164 release probability favors facilitation.<sup>33,35,36</sup> Thus, differences in postsynaptic responses to paired-  
165 pulse stimulation indicate variations in presynaptic transmitter release.<sup>33,36-38</sup> To probe the changes  
166 in efficacy of unitary ePSCs paired-pulse protocols were performed with short inter-stimulus  
167 interval (50 ms). Figure 2d shows representative presynaptic pairs of action potentials (top) and  
168 the corresponding monosynaptic GABAergic (left tracings) or glutamatergic AMPA receptor  
169 (right) evoked currents (bottom) before and after s-GO local pressure ejection. We indirectly  
170 assessed the GABA and glutamate release probability before and after saline (control) or s-GO  
171 ejection by measuring the paired-pulse ratio (PPR, calculating the ratio between the mean peak  
172 amplitude of the second and the first PSC<sup>37,38</sup>). In control GABAergic and glutamatergic ePSCs  
173 the resulting PPR indicated the presence of paired pulse depression and did not change upon saline  
174 solution applications (for GABA<sub>A</sub> receptor-mediated pairs:  $0.5 \pm 0.2$  before and  $0.6 \pm 0.2$  after  
175 saline; for AMPA receptor-mediated pairs:  $0.5 \pm 0.1$  before and  $0.6 \pm 0.2$  after saline, plot in Figure  
176 2d). When investigating the impact of s-GO ejection, we detected a reduction (on average – 32 %)

177 in the amplitude of the first glutamatergic ePSC and a significant difference (\*  $P < 0.05$  Student's  
178 t-test) in PPR, indicative of paired-pulse facilitation, while the PPR did not change in GABA<sub>A</sub>  
179 ePSCs (for AMPA mediated pairs:  $0.5 \pm 0.1$  before and  $2 \pm 0.9$  after s-GO; for GABA<sub>A</sub> mediated  
180 pairs:  $0.5 \pm 0.2$  before and  $0.65 \pm 0.2$  after s-GO; summarized in the bar plots in Figure 2d, bottom).  
181 Altogether these experiments strongly support a direct interference of s-GO flakes with synaptic  
182 vesicle release, with an initial high rate of release followed by a decline when s-GOs are applied  
183 longer<sup>10</sup> or when acting synergistically to the action potential-evoked activation of the exocytotic  
184 apparatus, ultimately depleting evoked release, typically reflected by changes in ePSC  
185 amplitude.<sup>39,40</sup> Notably, only glutamatergic synapses were targets of the s-GO.

186 **s-GO exposure specifically affects glutamatergic synapses in acute hippocampal slices.** Since  
187 cultured networks are simplified 2D models of immature brain circuits, we explored the ability of  
188 s-GO to regulate glutamate synaptic activity in acute hippocampal slices, thus scaling up the  
189 complexity of the tissue to the third dimension and testing more mature synapses. Single neuron  
190 patch-clamp recordings were obtained from visually identified pyramidal cells in the CA1  
191 hippocampal region. A second pipette was again positioned at a distance of 200  $\mu\text{m}$  from the  
192 recorded cell (sketched in Figure 3a) and filled with standard saline solution or with s-GO (100  
193  $\mu\text{g}/\text{mL}$ ). Baseline PSCs were recorded before and after the local saline or s-GO ejection. Figure  
194 3b shows representative current tracings of controls (top) and s-GO (bottom) before and after  
195 saline or s-GO solutions, respectively, were pressure ejected. In neurons exposed to saline solution,  
196 spontaneous PSCs frequency did not change ( $6 \pm 2$  Hz before the pipette saline-ejection and  $5 \pm 1$   
197 Hz after the pipette saline-ejection,  $n = 14$ ). On the contrary, acute s-GO ejection significantly  
198 increased (\*  $P < 0.05$  Student's t-test) the PSCs frequency (from a baseline of  $5 \pm 2$  Hz to a post  
199 ejection frequency of  $8 \pm 2$  Hz,  $n = 13$ ). The increase in PSCs after the local s-GO ejection was

200 reversible. In fact, PSC frequency fully returned to baseline values 7-8 min following the acute  
201 application. In all treatments, the PSC amplitude was not affected. We further dissected the nature  
202 of PSCs by the use of CNQX or Gabazine, isolating GABA<sub>A</sub> or AMPA receptor-mediated IPSCs  
203 or EPSCs, respectively. When EPSCs were measured after s-GO ejection, we detected a strong  
204 increase (\* P < 0.05 Student's t-test) in their frequency when compared to the saline solution  
205 pressure application ( $4 \pm 1$  Hz before and  $4.7 \pm 1$  Hz after the pipette saline-ejection;  $4.2 \pm 0.9$  Hz  
206 before and  $7.3 \pm 1$  Hz after the s-GO ejection, Figure 3c). On the contrary, when we measured  
207 IPSCs, their frequency was not affected both by saline ( $4.2 \pm 1$  Hz before and  $4.8 \pm 1$  Hz after,  
208 Figure 3d) and s-GO ( $3.8 \pm 1$  Hz before and  $4.2 \pm 1$  Hz after, Figure 3d) pressure applications.  
209 Such results support the notion of s-GO ability to specifically target excitatory synapses, even in  
210 tissue explants. In cultured neurons as well as in acute hippocampal slices, the brief pressure  
211 ejection of s-GO transiently increased the excitatory activity, apparently affecting glutamate  
212 release machinery at the presynaptic site.

213 To ascertain whether prolonged interference of s-GO with excitatory synapses might indeed  
214 reduce the activity of synapses capable of releasing glutamate, as observed in dissociated cultures<sup>10</sup>  
215 we incubated acute slices with s-GO (50  $\mu$ g/mL) and we monitored PSCs frequency after 30 min  
216 (n = 5), 45 min (n = 5), 3 h (n = 5) and 6 h (n = 8). Under these experimental conditions, s-GO  
217 will be repeatedly presented at synapses, in the absence of the fast clearance brought about by  
218 saline flow rate in the previous experiments (see Methods). The plots in Figure 3e compare the  
219 frequencies of PSCs in Control and s-GO treated samples against 4 different exposure time points.  
220 A progressive reduction in PSCs frequency was observed from 30 min to 6 h (from  $5.8 \pm 1$  Hz to  
221  $3.6 \pm 0.8$  Hz), such changes were not detected in control (from  $5.0 \pm 1$  Hz to  $5.3 \pm 1$  Hz). In Figure  
222 3e, by linear regression analysis of the two time progressions (Control and s-GO) combined to

223 multiple regression statistical analysis, we show that the zero slope hypothesis is accepted for  
224 Controls but not for s-GO, indicative of a significant progressive decrease in PSCs frequencies due  
225 to s-GO prolonged incubation.

226 **In vivo intra-hippocampal s-GO delivery reversibly reduces glutamatergic synaptic activity**

227 **in juvenile rats with minimal tissue reaction.** To gain more insights into the synapse specificity,

228 tissue reactivity and kinetics of s-GO in vivo, we injected in juvenile rats (P15) 1  $\mu$ L of s-GO (50

229  $\mu$ g/mL in saline solution; Figure 3f) in the dentate gyrus of the hippocampus and we patch-clamped

230 single neurons to measure glutamatergic synaptic activity from ex vivo hippocampal slices isolated

231 after 48 h and 72 h after the brain surgeries. As control, we injected 1  $\mu$ L of saline solution in the

232 same anatomical region. Figure 3f shows representative current tracings of the recorded electrical

233 activity in acute slices isolated from the contralateral (not subjected to the injection), the control

234 saline- and s-GO-injected hemispheres, after 48 h from injection. After this time period

235 hippocampal slices isolated from s-GO treated animals showed a clear and significant (\*\*  $P < 0.01$

236 two-way ANOVA) reduction in PSCs frequency ( $2 \pm 0.5$  Hz,  $n = 7$ ), when compared with slices

237 from the contralateral untreated hemisphere ( $5 \pm 1$  Hz,  $n = 9$ ) or with saline treated ones ( $4.3 \pm 1$

238 Hz,  $n = 8$ ; see plot in Figure 3g). Remarkably, such effects were reversible: upon 72 h recovery

239 post injections the reduction in synaptic PSCs frequency in s-GO treated slices is absent ( $6 \pm 1.3$

240 Hz,  $n = 8$  for contralateral slices;  $5.7 \pm 1.5$  Hz,  $n = 7$  for saline-injected slices;  $6.2 \pm 1.8$  Hz,  $n = 7$

241 for s-GO-injected slices; see plot in Figure 3g). In all treatments, the PSCs amplitude was not

242 affected. When pharmacologically discriminating GABA<sub>A</sub> and AMPA receptor-mediated PSCs,

243 we specifically detected after 48 h of s-GO a significant (\*  $P < 0.05$  two-way ANOVA) reduction

244 in EPSCs frequency ( $2.9 \pm 0.8$  Hz,  $n = 7$ ), when compared with slices from the contralateral

245 untreated hemisphere ( $4.8 \pm 1$  Hz,  $n = 9$ ) or with saline treated ones ( $5 \pm 1.3$  Hz,  $n = 8$ ; see right

246 plot in Figure 3h). GABA<sub>A</sub> receptor-mediated PSCs were not affected by any treatment (from  $3.5$   
247  $\pm 1$  Hz to  $3.9 \pm 0.8$  Hz after saline-ejection,  $n = 8$ , and from  $3 \pm 0.5$  Hz to  $3.4 \pm 0.5$  Hz after s-GO-  
248 ejection;  $n = 7$ ). To prove the presence of s-GO and gain more insight regarding its fate within the  
249 hippocampus *in vivo*, we used bright field microscopy with correlative Raman based mapping  
250 (Figure 4a). Forty-eight h following intra-hippocampal delivery ( $50 \mu\text{g/mL}$  final concentration;  $1$   
251  $\mu\text{L}$  injected volume), the presence of s-GO could be positively identified within the  $20 \mu\text{m}$  sections  
252 of injected hippocampi, specifically within the confines of the dentate gyrus. However,  $72$  h post  
253 injection, the material presence is shown to decrease. We also tested the hippocampi of rats that  
254 were injected with a saline control and a higher concentration of s-GO ( $1.3 \text{ mg/mL}$ ;  $1 \mu\text{L}$ ), which  
255 served as negative and positive controls, respectively, to verify our data. The localization of s-GO  
256 by using QD-s-GO ( $50 \mu\text{g/mL}$ ;  $1 \mu\text{L}$ ) was performed next. Figure 4b shows the  
257 immunofluorescence labeling of slices isolated from the treated hippocampus where the area of  
258 injection is highlighted by the typical microglia reaction (Iba1 positive cells in green) due to the  
259 surgery *per se*.<sup>41,42</sup> QD-s-GO was typically localized in the area of injection after  $24$  h (red  
260 staining). Next we investigated whether s-GO injection was affecting the number of synapses in  
261 the injected brain area. We used bassoon marker for pre-synaptic terminals present in both  
262 glutamatergic and GABAergic synapses.<sup>29</sup> We quantified the co-localization of bassoon with  
263 neurons (labeled with  $\beta$ -tubulin III) and we did not detect any difference between saline and s-GO  
264 treated ( $48$  h) animals in terms of bassoon volume at the injection site (saline  $552.68 \pm 155.06 \mu\text{m}^3$   
265 and s-GO  $570.40 \pm 115.74 \mu\text{m}^3$ ; number of animals =  $2$  for each experimental group; Figure 4c,d).  
266 To investigate tissue reactivity, in particular neuroglia responses, to s-GO following  $48$  h and  $72$   
267 h, we performed immunohistochemistry experiments on treated animals to identify GFAP-positive  
268 astrocyte and Iba1-positive microglia (number of animals =  $3$  for each experimental group; Figure

269 5a,b). We measured astrocytes and microglia located 300  $\mu\text{m}$  apart to the injection site in the  
270 medial and lateral directions, at such a distance we detected only a low tissue response in all groups  
271 (Figure 5c,d). Conversely, at the injection site the tissue reactivity was higher, as expected,<sup>41,42</sup> yet  
272 comparable between saline and s-GO. To note, astrocyte recruitment was decreased in s-GO  
273 treated animals, particularly after 48 h; while microglia reactivity was similar in saline and s-GO  
274 groups after 48 h, but it was significantly lower in s-GO treated animals after 72 h (Figure 5; \*\*  
275  $P < 0.01$ ; two-way ANOVA).

276 We report here the ability of s-GO nanosheets to interact selectively with glutamatergic synapses,  
277 affecting the efficacy of neurotransmission, *in vitro* and *in vivo*. In particular, in cultured  
278 hippocampal neurons, brief exposures to s-GO promote an initial high rate of glutamate quantal  
279 release, presumably by modifications at the pre-synaptic site, as indicated by the increase in  
280 frequency of spontaneous mEPSCs<sup>25,43,44</sup> and by the paired-pulse experiments.<sup>33,35-38</sup> We  
281 hypothesize that this initial high rate of release depletes presynaptic glutamate and, in the  
282 continuous presence of s-GO, inhibit glutamatergic transmission. Indeed, in the same preparation,  
283 the decline in action potential-evoked monosynaptic EPSCs upon s-GO exposure supports the  
284 notion of a subsequent reduction in the probability of release following vesicle depletion<sup>45</sup> brought  
285 about by s-GO. In all tests, the mere pressure ejection of saline solution without s-GO, or GO of  
286 different dimensions, did not change spontaneous or evoked synaptic responses. Notably,  
287 GABAergic synapses were never affected. The bi-phasic effects of s-GO, characterized first by a  
288 transient increase in neurotransmitter release which, upon a potential reduction in the vesicle-pool  
289 size, is followed by a depression, hints at the ability of s-GO to engage the presynaptic exocytotic  
290 machinery, as also supported by the co-localization with pre synaptic terminal markers.  
291 Neurotransmitter release, at the presynaptic site in the CNS, is controlled by specific proteins that

292 function in large complexes, displaying multiple roles in synaptic vesicle recycling.<sup>46</sup> In addition  
293 to release-proteins another potential target of s-GO is represented by intracellular  $\text{Ca}^{2+}$  levels,  
294 known to regulate evoked neurotransmitter release<sup>45</sup> and recently reported to be modulated by  
295 chronic exposure to s-GO.<sup>47</sup> Although we cannot exclude a role of presynaptic  $\text{Ca}^{2+}$  influx  
296 contributing to acute s-GO effects, the detected increase in spontaneous miniature current  
297 frequency, much less dependent on  $\text{Ca}^{2+}$  levels,<sup>44,48</sup> and the absence of modulation by s-GO of the  
298 GABAergic terminals, usually regulated by presynaptic  $\text{Ca}^{2+}$  dynamics<sup>49</sup>, are suggestive of a  $\text{Ca}^{2+}$   
299 independent mechanisms. The responses evoked by pressure ejected s-GO are reminiscent to those  
300 induced by hypertonic solutions<sup>50</sup>, however a simple osmotic mechanism is ruled out by the  
301 selectivity of the effects (restricted to glutamatergic terminals) observed in all conditions tested  
302 and by direct osmotic pressure measures (see Methods). The current data are in agreement with  
303 our previous report, where a long-term (days) exposure to s-GO selectively down regulated  
304 excitatory neurotransmission leaving inhibitory synapses unchanged.<sup>10</sup> We previously  
305 speculated<sup>10</sup> that differences in GABAergic and glutamatergic synaptic cleft ultrastructure, in  
306 particular in the cleft size and organization<sup>51</sup>, might explain why the latter terminals became ideal  
307 targets to s-GO interactions. To note, larger or smaller GO flakes did not modulate glutamate-  
308 mediated synaptic transmission. In this framework, we propose a simply mechanistic interpretation  
309 of our current experiments: glutamatergic synapses, in virtue of their relatively larger size and less  
310 structured organization,<sup>51</sup> allow penetration of s-GO flakes which remain trapped within the cleft  
311 and adhere to the plasma membrane at active release sites. GO nanosheets have been suggested to  
312 adhere to complex patches of cellular membranes, rather than specific ones.<sup>52</sup> Also in our  
313 experiments, the s-GO adhesion to the membrane may be supported by non-specific interactions  
314 (as described in other cell types<sup>52</sup>) accompanied by variable degrees of membrane deformations, a

315 mechanism further supported by our previous results showing astrocyte vesicle shedding when  
316 exposed to s-GO.<sup>10</sup> A deformation of synaptic active zones would interfere with the exocytosis  
317 and neurotransmitter vesicle release by a mechanical mechanism reminiscent of, for example,  
318 stress induced ones,<sup>50</sup> not necessarily implying an impairment of membrane integrity. In fact, we  
319 never observed any functional sign of membrane damage, and in addition the alterations in vesicle  
320 release were reversible. An alternative mechanism, due to the physical properties of nanoparticles,  
321 is related to their surface potential, able to tune neuronal excitability.<sup>53</sup> We previously documented  
322 that the s-GO surface potential, measured as zeta potential value<sup>10</sup>, is negative ( $-50$  mV), thus the  
323 negative charge may favor the s-GO interactions with neuronal membrane influencing the  
324 excitability of neurons.<sup>53</sup> Although we cannot exclude this mechanism, the short- and long- term  
325 regulation and the selectivity for excitatory synapses are not explained by this interpretation. The  
326 interface between dispersed s-GO sheets and the cell membrane is currently subject to active  
327 investigation, due to its potential in modulating cellular mechanosensing for diverse biomedical  
328 applications, nevertheless the nature of such interactions is still elusive.<sup>52,54</sup> Synaptic vesicle  
329 recycling machinery represents a feasible therapeutic target, regardless of the direct involvement  
330 of presynaptic function in a pathological process. Even subtle alterations in (pre)-synaptic  
331 communication hold the potential to compensate for deficits without interfering with postsynaptic  
332 signaling. Pre-synaptically targeted drug development might be challenging due to the  
333 sophisticated molecular complexity of the release machinery. The ability of s-GO to specifically  
334 hook glutamatergic presynaptic nerve terminals is thus highly promising, however conventional  
335 2D cultures may lack appropriate cell-extracellular matrix interactions, providing an artificially  
336 higher access of exogenous agents to synapses. s-GO specificity towards glutamatergic synapses  
337 may be virtually restricted to 2D bio-system models. This potential pitfall is excluded by our

338 experiments on acute hippocampal slices, the neuroscientist gold standard to investigate synaptic  
339 functions in intact circuitries. The selective effect of s-GO on glutamatergic transmission is  
340 preserved in tissue slices, where excitatory EPSCs are reversibly affected by s-GO, with a short-  
341 term up-regulation of release, turned into a down regulation upon prolonged exposure. The  
342 ultimate potential of any s-GO sheets in the design of therapeutic strategies based on synaptic  
343 targeting resides in testing their efficacy in vivo. We demonstrated the delivery of s-GO in vivo  
344 by stereotactic injection and we have shown that such an administration of s-GO (but not the  
345 surgery per se) in the hippocampus of juvenile rats significantly and selectively sized down  
346 glutamatergic activity, in the absence of direct reduction in the number of synapses. We have also  
347 shown that local tissue responses to stereotactic injections<sup>41,42</sup> were not increased by the presence  
348 of s-GO in terms of patterns of microglia together with astrocyte aggregation at the injection site.  
349 These results are supportive of, within the concentrations tested, the in vivo biocompatibility of  
350 the s-GO dispersions. In general, GO is characterized by better biocompatibility when compared  
351 to other types of graphene (such as pristine graphene or reduced GO) and additional  
352 functionalization might even further reduce the risk of inflammation and subsequent tissue  
353 toxicity.<sup>55</sup> Interestingly, our results also suggest a possible anti-inflammatory effect by limiting the  
354 aggregation of astrocytes surrounding the stereotactic injection and lessening prolonged microglia  
355 reactivity.<sup>41,42</sup> This result, although preliminary, is in accordance with previous observations<sup>56</sup> and  
356 renders further investigation. Exploiting s-GO in pre-synaptic drug design development certainly  
357 requires additional studies, as well as to ascertain a more precise s-GO mechanism of action and  
358 clearance, since in our experiments, due to diffusion, perfusion flow rate in vitro, potential  
359 membrane recycling,<sup>57</sup> and microglial uptake<sup>58</sup> we probably had only a “local” tissue clearance.  
360 Besides, most of the studies evaluating the clearance in vivo of GO suggested that GO is rapidly

361 cleared, but have been performed in non-mammalian organisms.<sup>59,60</sup> In our proof-of-concept  
362 vivo study the coherence between the low detection of residual s-GO at 72 h and the reversibility  
363 of the synaptic silencing upon 72 h are supportive of a direct, mechanical interaction at the pre-  
364 synaptic plasma membrane.

## 365 **Methods**

366 **Graphene oxide nanosheets synthesis.** GO was manufactured under endotoxin-free conditions  
367 through our modified Hummers' method as previously described.<sup>10,61</sup> Briefly in this procedure, 0.8  
368 g of graphite flakes was added to 0.4 g of sodium nitrate (Sigma-Aldrich, UK). This was next  
369 followed by the slow addition of 18.4 mL of sulfuric acid 99.999% (Sigma-Aldrich, UK). After a  
370 homogenized mixture was achieved through stirring, 2.4 g of potassium permanganate (Sigma-  
371 Aldrich, UK) were added and maintained for 30 min. Thereafter, 37 mL of water for injection  
372 (Fresenius Kabi, UK) were added. This resulted in an exothermic reaction. The temperature was  
373 strictly kept at 98 °C for 30 min. The mixture was next diluted with 112 mL of water for injection  
374 (Fresenius Kabi, UK). Twelve mL of 30% hydrogen peroxide (Sigma-Aldrich, UK) were then  
375 added to reduce the residual  $\text{KMnO}_4$ ,  $\text{MnO}_2$ , and  $\text{MnO}_7$  to soluble manganese sulphate salts. The  
376 resulting mixture purified by repeated centrifugation cycles at 9000 rpm for 20 min until an  
377 orange/brown gel-like layer of GO began to appear on at the pellet-supernatant interface which  
378 occurred at around pH 6-7. This layer was carefully extracted with warm water for injection  
379 (Fresenius Kabi, UK). This layer contained large GO sheets; the obtained material was diluted in  
380 water for injection to yield an aqueous suspension with a concentration of 2 mg/mL. A portion of  
381 this obtained material was then lyophilised, reconstituted in water for injection (Fresenius Kabi,  
382 UK) and then sonicated in a bath sonicator (VWR, 80W) for 5 min. The resulting dispersion was  
383 then centrifuged at 13000 rpm for 5 min at room temperature (RT); the supernatant which

384 contained the desired s-GO nanosheets was separated from the unwanted pellet. A thorough  
385 physico-chemical characterization of us-GO and l-GO has already been reported.<sup>18</sup> Structural  
386 properties such as lateral dimension and thickness of the GO materials were then studied by AFM  
387 and TEM. Raman spectroscopy and  $\zeta$ -potential measurements were used to define the materials  
388 surface properties. TGA was also performed to examine the functionalization degree of the s-GO  
389 sheets. Moreover, XPS was used to examine the composition of the GO sheets, C/O ratio, and the  
390 presence of the different functional groups.

391 **s-GO functionalization.** QD have been prepared according to the literature by controlled  
392 decomposition of Ag and In salts. Briefly, 88.4 mg of  $\text{InCl}_3$  (0.4 mmol, Sigma Aldrich) and 17 mg  
393  $\text{AgNO}_3$  (0.1 mmol, Sigma Aldrich) were placed in a 100 ml round-bottom flask. Then, 190  $\mu\text{L}$  of  
394 oleic acid (0.6 mmol, Sigma Aldrich), 720  $\mu\text{L}$   $\square\square\square\square$  dodecylthiol (0.6 mmol, Sigma Aldrich) and  
395 8 mL of 1-octadecene (Sigma Aldrich) have been added under argon. The solution was heated at  
396 60 °C for 15 min, at 90 °C for 15 min, and left at 110 °C stirring till no precipitate was visible (15-  
397 30 min). Then, 4 mL of solution S (9.6 mg 0.3 mmol, Sigma Aldrich) was added and the mixture  
398 turned reddish. Finally, 5 mL of  $\text{ZnCl}_2$  solution (70.5 mg 0.5 mmol, Sigma Aldrich) in oleylamine  
399 and 1-octadecene were added and the temperature was raised to 150 °C. After 15 min, the reaction  
400 was cooled with an ice bath. The QDs were purified by precipitation with ethanol, re-suspended  
401 with cyclohexane, washed several times with ethanol/acetone and stored in  $\text{CH}_2\text{Cl}_2$ . For the water  
402 transfer reaction, 2 mL of solution oil QDs (2 mg/mL dispersion) have been added to 1 mL of a  
403 cysteine (50 mg 0.4 mmol) basic solution in methanol. Immediately, the QD precipitated. After 20  
404 min, 5 mL of distilled water have been added and the QD passed through the aqueous phase.  
405 Subsequently, the water soluble QDs have been precipitated with acetone, washed several times  
406 with acetone/ethanol and stored in distilled water. For GO conjugation QDs have been mixed with

407 GO (1 mg/mL) at 1/10 mass ratio in distilled water. The mixture has been left stirring for 3 days  
408 and then purified via dialysis against distilled water.

409 **Preparation of hippocampal cultures and acute hippocampal slices.** Primary hippocampal  
410 cultures were prepared from neonatal rats at 2-3 postnatal days (P<sub>2</sub>-P<sub>3</sub>) as previously  
411 reported.<sup>10,26,62</sup> All procedures were approved by the local veterinary authorities and performed in  
412 accordance with the Italian law (decree 26/14) and the UE guidelines (2007/526/CE and  
413 2010/63/UE). The animal use was approved by the Italian Ministry of Health. All efforts were  
414 made to minimize suffering and to reduce the number of animals used. All chemicals were  
415 purchased by Sigma-Aldrich unless stated otherwise. Cultures were then used for experiments  
416 after 8 ÷ 12 days in vitro. Hippocampal acute slices were obtained from P<sub>7</sub>-P<sub>8</sub> rats and from  
417 juvenile P<sub>15</sub> rats (n = 18 animals) using a standard protocol.<sup>63,64</sup>

418 **Electrophysiological recordings.** In dissociated hippocampal cultures, single and paired whole-  
419 cell recordings were obtained with pipettes (5-7 MΩ) with the following intracellular saline  
420 solution (in mM): 120 K gluconate, 20 KCl, 10 HEPES, 10 EGTA, 2 MgCl<sub>2</sub>, 2 Na<sub>2</sub>ATP, pH 7.3;  
421 osmolarity 300 mOsm. The extracellular saline contained (in mM) 150 NaCl, 4 KCl, 1 MgCl<sub>2</sub>, 2  
422 CaCl<sub>2</sub>, 1 MgCl<sub>2</sub>, 10 HEPES, 10 glucose, pH 7.4. Data were recorded by Multiclamp 700B patch  
423 amplifier (Axon CNS, Molecular Devices) digitized at 10 KHz by pClamp 10.2 software  
424 (Molecular Devices LLC, USA). Basal PSCs were recorded at -56 mV holding potential (liquid  
425 junction potential of 14 mV was not corrected for). mPSCs were recorded in the presence of TTX  
426 (1 μM) to block fast voltage-dependent sodium channels. In voltage-clamp recordings, PSCs and  
427 mPSCs were detected by the use of the AxoGraph X (Axograph Scientific) event detection  
428 program and by the Clampfit 10 software (pClamp suite, Axon Instruments) as previously  
429 reported<sup>64</sup>. On average, ≥ 500 PSCs were analyzed from each cell and from the average of these

430 events we measured the peak amplitude and the decay time constant (expressed as  $\tau$ ) by fitting a  
431 mono-exponential function. In paired recordings, the presynaptic neuron in current clamp mode  
432 was held at  $-70$  mV (by  $\leq 0.02$  nA negative current injection), and action potentials were evoked  
433 by delivering short (4 ms) square current pulses (1 nA). Monosynaptic connections were identified  
434 by their short delay ( $< 2$  ms)<sup>64</sup>. To characterize the short-term dynamics of synaptic contacts, we  
435 delivered, to pairs of connected neurons, paired pulse stimulations at 20 Hz (1 pair every 20 s; 10  
436 times, that were pooled together and averaged). For acute hippocampal slices, a patch-clamp  
437 amplifier (Multiclamp 700B, Axon Instruments, Sunnyvale, CA, USA) allowed recordings from  
438 CA1 pyramidal neurons, identified by visual inspection at an upright microscope (Eclipse FN1;  
439 Nikon, Japan) equipped with differential interference contrast optics and digital videocamera  
440 (Nikon, Japan). All recorded events were analyzed offline with the AxoGraph 1.4.4 (Axon  
441 Instrument) event detection software (Axon CNS, Molecular Devices). s-GO was acutely  
442 delivered<sup>10</sup>, both in dissociated cells and in acute hippocampal slices, by an injection of pressurized  
443 air (500 ms duration, 8 PSI; by a Picospritzer PDES-02DX; NPI electronic GmbH, Germany).  
444 Once patch-clamped neurons, a second pipette identical to that used for patch-clamp recording,  
445 was positioned at a distance of 200  $\mu\text{m}$  (under microscopy control) from the recorded cell. The  
446 pipette was filled with standard saline solution (control; osmolarity 300 mosmol  $\text{l}^{-1}$ ) or with s-GO,  
447 l-GO and us-GO (100  $\mu\text{g}/\text{mL}$  in Krebs solution; osmolarity 300 mosmol  $\text{l}^{-1}$ ). The concentration of  
448 GO reaching the cell was at least 10 % of that contained in the pipette, considering 1 mL of  
449 extracellular solution in the recording chamber. Baseline PSCs were sampled before (10 min) and  
450 after (10 min) the local ejection. Analyses were performed between 4 min and 8 min after the local  
451 ejection, sampling 2 min of recordings.

452 **Confocal microscopy in hippocampal cultures.** Cultured hippocampal neurons (3 cultures; 6-8  
453 DIV) were incubated for 30 minutes with s-GO (20  $\mu\text{g}/\text{mL}$ ). Cultures were then fixed by 4 %  
454 formaldehyde (prepared from fresh paraformaldehyde; Sigma) in PBS at RT and blocked and  
455 permeabilized in 5 % fetal bovine serum (FBS), 0.3 % Triton-X 100 in PBS for 30 min at RT.  
456 Samples were incubated with primary antibodies (mouse monoclonal anti-bassoon, 1:400 dilution;  
457 rabbit anti- $\beta$ -tubulin III, 1:500 dilution) diluted in PBS with 5 % FBS for 45 minutes. Cultures  
458 were finally incubated with secondary antibodies (Alexa 488 goat anti-mouse, Invitrogen, 1:500  
459 dilution; Alexa 594 goat anti-rabbit, Invitrogen, 1:500 dilution) and DAPI (Invitrogen, dilution  
460 1:200) to stain the nuclei, for 45 minutes at RT and finally mounted on 1 mm thick glass coverslips  
461 using the Fluoromount mounting medium (Sigma-Aldrich). To visualize s-GO localization was  
462 used the reflection mode of confocal microscopy.<sup>58</sup> Images were acquired using a Nikon C2  
463 Confocal, equipped with Ar/Kr, He/Ne and UV lasers. Images were acquired with a  $60\times$  (1.4 NA)  
464 oil-objective (using oil mounting medium, 1.515 refractive index). Confocal sections were  
465 acquired every 0.4  $\mu\text{m}$ .

466 **Surgery and s-GO injection.** Four experimental groups were used: standard saline solution  
467 (control) and s-GO 50  $\mu\text{g}/\text{mL}$  injection, analyzed at 48 h and 72 h. Surgery was performed in P<sub>15</sub>  
468 Wistar rats anesthetized with ketamine (60 mg/kg i.p.) and xylazine (10 mg/kg i.p.). All animal  
469 procedures were conducted in accordance with the National Institutes of Health, international and  
470 institutional standards for the care and use of animals in research, and after consulting with a  
471 veterinarian. All experiments were performed in accordance with the EU guidelines (2010/63/UE)  
472 and Italian law (decree 26/14) and were approved by the local authority veterinary service. All  
473 efforts were made to minimize animal suffering and to reduce the number of animal used. The  
474 Italian Ministry of Health, in agreement with the EU Recommendation 2007/526 /CE, approved

475 animal use (authorization n° 1135/2015-PR). Animals were fixed in a stereotaxic device (World  
476 Precision Instruments, WPI). An incision was made on the top of the head in order to expose the  
477 skull and identify bregma and lambda coordinates. The injection of 1  $\mu$ L of saline or s-GO solution  
478 (10 steps of 0.1  $\mu$ L every minute) was performed with a Hamilton syringe (26s gauge; Hamilton).  
479 The following coordinates were used to reach the left dentate gyrus: AP: -3.0, ML: -3.0, DV: -3.3  
480 relative to bregma.<sup>65</sup> At the end of the last step, the syringe was left in situ for extra 5 minutes to  
481 optimize the solution permeation. The incision was sutured and animals were constantly monitored  
482 and left undisturbed until electrophysiological or histological experiments.

483 **Histology procedures.** After 48 h or 72 h, animals were anesthetized and sacrificed by intracardiac  
484 perfusion with 0.1 M PBS followed by 4 % formaldehyde (prepared from fresh paraformaldehyde;  
485 Sigma) in PBS. Brains were promptly removed, postfixed in the same fixative solution for 24 h at  
486 4 °C, and cryoprotected in 30 % sucrose in PBS at 4 °C for 24-48 h. Finally, brains were embedded  
487 in optimal cutting temperature (OCT) compound (Tissue-Tek), frozen at – 20 °C, and sagittal  
488 sections (25  $\mu$ m) were obtained using a cryostat (Microm HM 550, Thermo Fisher Scientific) and  
489 processed for immunohistochemistry. Tissue-Tek was removed by PBS washing and tissue  
490 sections were protein-blocked in 3 % BSA, 3 % FBS and 0.3 % Triton X-100 in PBS for 45 minutes  
491 at RT. Sections were then incubated overnight at 4 °C with primary antibodies (mouse anti-GFAP,  
492 Sigma-Aldrich, 1:400; rabbit anti-Iba1, Wako, 1:500; rabbit anti- $\beta$ -tubulin III, Sigma-Aldrich,  
493 1:500; mouse anti-Bassoon, Abcam, 1:400) in 5 % FBS in PBS. After washing in PBS, sections  
494 were incubated in secondary antibodies (goat anti-rabbit AlexaFluor 594, Thermo Fisher  
495 Scientific, 1:400; goat anti-mouse AlexaFluor 488, Thermo Fisher Scientific, 1:400) in 5% FBS  
496 in PBS for 2-4h at RT. Nuclei were labeled with DAPI (Thermo Fisher Scientific, 1:500) in PBS

497 for 20-30 minutes at RT. Upon final washing (PBS and water), tissue sections were mounted on  
498 glass coverslips using Vectashield mounting medium (Vector Laboratories).

499 **Image acquisition and analysis.** We measured the brain tissue reaction by markers for reactive  
500 astrocytes and microglia (GFAP and Iba1, respectively). Fluorescence images were acquired using  
501 a Leica DM6000 upright microscope with a 10 × dry objective. Identical binning, gains and  
502 exposure times were used for all images of the same marker. Image analysis was performed using  
503 Fiji software. For both GFAP and Iba1 intensity measurements, a single region of interest (ROI,  
504 1000 × 500 μm<sup>2</sup>) was selected at the injection site (left dentate gyrus). The background intensity  
505 threshold was defined for each section using the labeling intensity measured in the contralateral  
506 hemisphere in the same anatomical region (right dentate gyrus). The area within each ROI with  
507 intensity above the background threshold was calculated, normalized to the contralateral  
508 hemisphere and used for statistics. The ROI for all sections were averaged for each experimental  
509 group. We performed this analysis also 300 μm medial and lateral to the injection site. We  
510 visualized s-GO by linking QD. Fluorescence images were acquired using a Leica DM6000  
511 upright microscope with a 10 × dry objective. We further analyzed the amount of synaptic contacts  
512 by a specific marker for synapses (bassoon) in two experimental groups: saline and s-GO injection  
513 at 48 h. Confocal images were acquired using a confocal microscope (Nikon C1) with a 60 × oil  
514 objective (N.A. 1.4, oil mounting medium refractive index 1.515). Z-stacks were acquired every  
515 350 nm for a total thickness of 7 μm. Identical binning, gain and exposure time was used for all  
516 images. 9 ROIs (70 × 70 μm<sup>2</sup>) for each section were randomly selected at the injection site (left  
517 dentate gyrus). Offline analysis was performed using Volocity software (Volocity 3D image  
518 analysis software, PerkinElmer, USA). For each ROI, we used the Z-stack to quantify bassoon  
519 signal as 3D objects. From the resulting values, we calculated the volume of only bassoon objects

520 co-localized with the  $\beta$ -tubulin III labeling in order to identify genuine synapses at neuronal level.

521 The ROI for all sections were pooled together and averaged for each experimental group.

522 **Raman mapping of brain sections.** Raman mapping of sectioned brain samples was completed

523 using a DXRi Raman Mapping system (Thermo Scientific, USA) using the following conditions:

524  $\lambda = 633$  nm, 1 mW, pixel size = 1.6  $\mu$ m and frequency = 25 Hz. The maps were generated according

525 to the composite spectra's percentage similarity to a correlation GO spectral reference as shown.

526 **Statistical analysis.** All values from samples subjected to the same experimental protocols were

527 pooled together and results are presented as mean  $\pm$  S.D., if not otherwise indicated; n = number

528 of neurons, if not otherwise indicated. Statistically significant difference between two data sets

529 was assessed by Student's t-test for parametric data. Differences between the logarithmic values

530 of the analyzed variables were assessed using two-way ANOVA and multiple comparisons were

531 adjusted by Bonferroni or Holm-Sidak correction. Statistical significance was determined at  $P <$

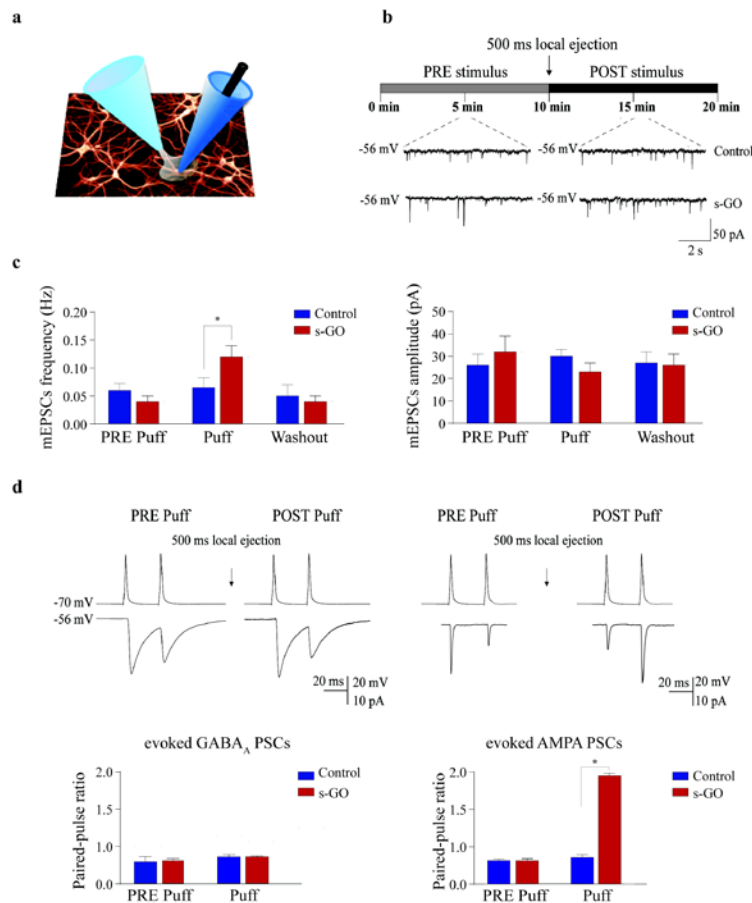
532 0.05, unless otherwise indicated. Significance was graphically indicated as follows: \* $P < 0.05$ , \*\* $P$

533  $< 0.01$ , \*\*\* $P < 0.001$ .

534

535

536 **Figure 1.** Characterization of s-GO. (a) AFM measure of s-GO sheets. (b) s-GO lateral  
537 dimension distribution. (c) S-GO Raman spectrum. (d) XPS survey of QD-s-GO. UV-vis (e) and  
538 fluorescence (f) spectra of s-GO, QD and QD-s-GO.



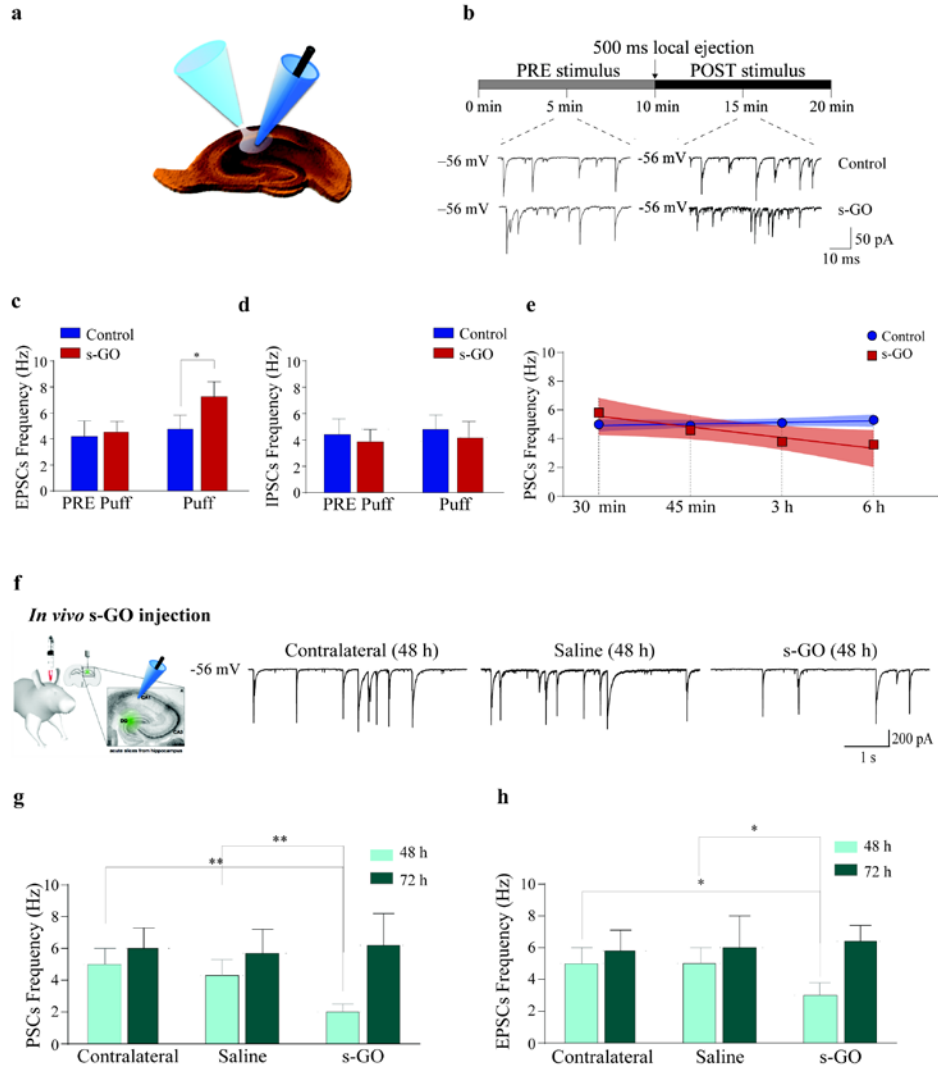
539

540 **Figure 2.** s-GO affects presynaptic glutamate release in hippocampal cultures (a) Sketch of the  
 541 experimental setting for simultaneous s-GO pressure-release (puff) and single-cell recording  
 542 from cultured neurons. (b) Top: diagram of the experimental protocol. Bottom: representative  
 543 tracings of the spontaneous synaptic activity detected prior and after puff applications of control  
 544 saline (Control, top) or s-GO (bottom). Recordings of mEPSCs are performed in the presence of  
 545 TTX. In (c) bar plots of pooled data summarize the average mEPSCs frequency (left) and  
 546 amplitude (right) before (PRE puff) and after (Washout) saline (Control) or s-GO (100  $\mu$ g/mL  
 547 final concentration) pressure ejections (\*  $P < 0.05$  Student's t-test). Note the reversible increase  
 548 in miniatures frequency due to s-GO. In (d) simultaneous pair recordings are shown: top traces  
 549 represent presynaptic pairs (30 Hz) of action potentials, bottom ones the corresponding evoked  
 550 monosynaptic PSCs (GABA<sub>A</sub>-receptor mediated on the left and glutamate AMPA-receptor  
 551 mediated on the right) prior and after s-GO puffs. The paired-pulse ratios (PPR) measured prior  
 552 and after saline solution (Control) and s-GO puffs are summarized in the histograms; note that s-

553 GO reduced the first evoked AMPA-receptor mediated PSCs and the PPR of glutamatergic  
554 synapses (\*P < 0.05 Student's t-test) supporting the notion of s-GO affecting presynaptic release.

555

556

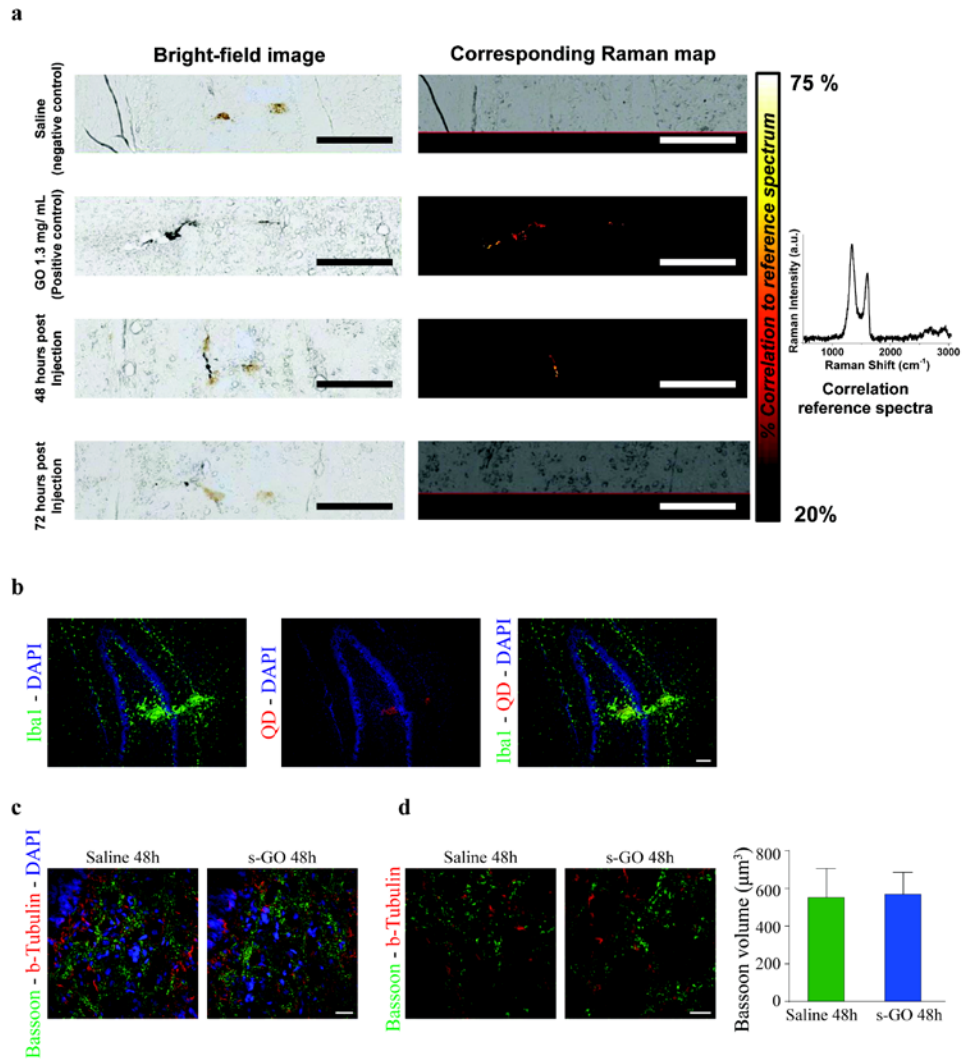


557

558 **Figure 3.** EPSCs frequency modulation by s-GO in hippocampal slices *in vitro* and *in vivo* (a)  
559 Sketch of the experimental setting for simultaneous s-GO release and recording from  
560 hippocampal pyramidal cells. In (b) top: diagram of the experimental protocol. Bottom:  
561 representative current tracings recorded prior and after saline (Control; top) and s-GO (bottom)  
562 local pressure ejections. Glutamate AMPA-receptor mediated PSCs or GABA<sub>A</sub>-receptor  
563 mediated ones (EPSCs and IPSCs, respectively) were pharmacologically isolated and bar plots in  
564 (c) summarize the mean values of EPSCs and in (d) of IPSCs frequency before and after saline  
565 (Control) or s-GO puffs (\*P < 0.05 Student's t-test). Note that also in hippocampal slice explants  
566 only glutamatergic activity was transiently affected by brief local injection of s-GO. In (e) plots  
567 of pooled data represent the average PSCs frequency upon 30 min, 45 min, 3 h and 6 h s-GO  
568 incubation (50 µg/mL final concentration; Control: blue circles; s-GO: red squares). Note that  
569 prolonged incubation in s-GO depresses spontaneous synaptic activity. Linear regression  
570 analysis of the two time progressions is depicted as blue and red fitting lines ( $y = 4.91 + 0.11x$  for  
571 Control and  $y = 5.56 - 0.74x$  for s-GO, respectively) together with their corresponding confidence  
572 interval in pale blue and pale red, respectively. Regardless the significance of the difference  
573 between each two conditions at a specific time point (at 30 m P = 0.91, at 45 m P = 0.60, at 3 h P  
574 = 0.07, at 6 h P = 0.06), multiple regression statistical analysis revealed that the zero slope  
575 hypothesis is accepted for Controls but not for s-GO. The equal slope hypothesis between the  
576 two trends was instead rejected by a Tukey test on the two slopes. f) *In vivo* intra-hippocampal s-  
577 GO delivery reversibly reduces glutamatergic synaptic activity in adult rats: sketch of the  
578 experimental settings (left) and (right) spontaneous synaptic activity recorded from *ex vivo*  
579 hippocampal slices isolated from juvenile rats after 48 h from the surgery. Recordings were  
580 taken from the contralateral, control (saline) and s-GO (50 µg/mL final concentration) injected  
581 hemisphere after 48 h from surgery. In (g) bar plots summarize the PSCs and in (h) the EPSCs  
582 frequency in control and s-GO treated animals after 48 h and after 72 h from surgery (\*\*P <  
583 0.001 two-way ANOVA; \*P < 0.05 two-way ANOVA). Note that the specific reduction in EPSC  
584 frequency at 48h that was entirely reversed at 72 h.

585

586



588 **Figure 4.** In vivo delivery of s-GO is localized and does not alter excitatory synaptic density. In  
589 (a) confocal Raman maps were acquired to establish the location of s-GO within cryosectioned  
590 dendate gyrus' of s-GO (1.3 mg/mL) treated animals over time (48 h and 72 h). Scale bars = 500  
591 nm. Maps were generated based on the acquired spectra's correlation to a s-GO reference spectra,  
592 shown on the right. The dentate gyrus of rats injected with saline (Controls) and rats treated with  
593 a higher concentration (1.3 mg/ mL) (positive control) were also examined for comparison. The  
594 acquisition parameters were as follows  $\lambda = 633$  nm, laser power = 1 mW, frequency = 25 Hz and  
595 a pixel size of 1.6  $\mu\text{m}$ . In (b) Ex vivo fluorescence imaging of hippocampal slices processed for  
596 Iba1-positive microglia (in green) and QD linked to s-GO (in red) at the injection site after 48 h.  
597 DAPI for nuclei is in blue. Note the precise localization of s-GO within the target area. (c) Ex  
598 vivo confocal images of hippocampal synapses at the injection site, excitatory presynaptic  
599 terminals were identified by the marker bassoon (in green), in neurons co-labeled with  $\beta$ -tubulin  
600 III (in red) and results are shown for saline (control) and s-GO injections after 48 h. DAPI for  
601 nuclei is in blue. Analysis has been performed at the higher magnification on  $70 \times 70 \mu\text{m}^2$  ROIs  
602 shown in (d) and results are summarized by the bar plots. No differences in bassoon  
603 quantification were detected between saline and s-GO injection after 48h. Scale bars: 100  $\mu\text{m}$  in  
604 (b), 25  $\mu\text{m}$  in (c) and 10  $\mu\text{m}$  in (d).

605

606

607

608

609 **Figure 5.** Brain tissue reactivity to surgery and s-GO injections after 48 h and 72 h. Ex vivo  
610 hippocampal slices from saline (control) and s-GO injected brains were labeled for GFAP-  
611 positive astrocytes (in green, top row) and Iba1-positive microglia (in red, bottom row) and the  
612 injection site (left dentate gyrus, saline vs. s-GO 50  $\mu\text{g}/\text{mL}$ ) are shown after 48 h (A) and 72 h  
613 (B). DAPI for nuclei is in blue. Scale bar: 100  $\mu\text{m}$ . Bar plots in (C) and (D) quantify the glial  
614 reaction 48 h and 72 h post- surgery. Comparable values of GFAP and Iba1 immunoreactivity  
615 between saline and s-GO were observed in the hippocampus at 300  $\mu\text{m}$  distance from the  
616 injection site, either lateral or medial in both 48 h and 72 h post-surgery. Notably, at the injection  
617 site, s-GO induced lower GFAP immunoreactivity at 48 h and lower Iba1 immunoreactivity at 72  
618 h when compared to controls. (\*\*  $P < 0.01$  two-way ANOVA).

619

620

621

622

## 623 ASSOCIATED CONTENT

624 Supplementary Information: Supplementary Figure 1; Supplementary Figure 2

625

626 **Corresponding Author**

627 #E-mail: laura.ballerini@sissa.it

628 #E-mail: kostas.kostarelos@manchester.ac.uk

629 **Author Contributions**

630 R.R. set up the experiments, performed and design electrophysiology and data analysis and  
631 contributed to the writing of the paper; M.M. performed the surgery, histology and confocal  
632 analysis; L.N. performed Raman spectroscopy and S.V. confocal microscopy, while both  
633 contributed to the writing of the results and methods; G.R and A.B. performed the synthesis and  
634 characterization of QD s-GO and contributed to the microscopy; M.P. contributed to the  
635 experimental design; K.K. contributed with synthesis and characterization of GO sheets,  
636 contributed to the experimental design and paper writing; L.B. conceived the idea, the  
637 experimental design and wrote the paper.

638 **Funding Sources**

639 We acknowledged financial support from the European Union's Horizon 2020 research and  
640 innovation program under grant agreements No. 696656 and No. 785219 Graphene Flagship

641

642 **ACKNOWLEDGMENT**

643 We thank E. Aurand for her help in setting the *in vivo* surgeries, A. F. Biagioni for help in  
644 performing histological analysis *in vivo*, M. Musto and G. Baj for the confocal microscopy at the

645 Light Microscopy Imaging Center (LMIC) of the University of Trieste-Life Sciences Department  
646 and A. F. Rodrigues for synthesis and characterization of GO sheets used in this study. D. Scaini  
647 is gratefully acknowledged for useful discussions.

## 648 REFERENCES

- 649 (1) Sanchez, V. C., Jachak, A.R., Hurt, H., Kane, A. B. Biological interactions of graphene-  
650 family nanomaterials: an interdisciplinary review. *Chem Res Toxicol.* **2012**, 25, 15-34.
- 651 (2) Kostarelos, K., Novoselov, K. S., Exploring the interface of graphene and biology. *Science.*  
652 **2014**, 18, 261-263.
- 653 (3) Mao, H. Y., Laurent, S., Chen, W., Akhavan, O., Imani, M., Ashkarran, A. A., Mahmoudi,  
654 M. Graphene: promises, facts, opportunities, and challenges in nanomedicine. *Chem Rev.* **2013**,  
655 8, 3407-3424.
- 656 (4) Novoselov, K. S., et al., Electric field effect in atomically thin carbon films. *Science* **2004**,  
657 306, 666–669.
- 658 (5) Geim, A. K. Graphene: status and prospects. *Science* **2009**, 324, 1530–1534.
- 659 (6) Guo, S., & Dong, S. Graphene nanosheet: synthesis, molecular engineering, thin film,  
660 hybrids, and energy and analytical applications. *Chem. Soc. Rev.* **2011**, 40, 2644–2672.
- 661 (7) Novoselov, K. S., et al., Two-dimensional atomic crystals. *Proc. Natl. Acad. Sci. U. S. A.*  
662 **2005**, 102, 10451–10453.
- 663 (8) Bitounis, D., Ali-Boucetta, H., Hong, B. H., Min, D. H., Kostarelos, K. Prospects and  
664 challenges of graphene in biomedical applications. *Adv. Mater.* **2013**, 25, 2258–2268.
- 665 (9) Kuzum, D., et al., Transparent and flexible low noise graphene electrodes for simultaneous  
666 electrophysiology and neuroimaging. *Nat. Commun.* **2014**, 5, 5259.
- 667 (10) Rauti, R., et al., Graphene oxide nanosheets reshape synaptic function in cultured brain  
668 networks. *ACS Nano.* **2016**, 10, 4459-71.
- 669 (11) Behar, T. N., et al., Glutamate acting at NMDA receptors stimulates embryonic cortical  
670 neuronal migration. *J. Neurosci.* **1999**, 19, 4449-4461.
- 671 (12) Fonnum, F. Glutamate: a neurotransmitter in mammalian brain. *J. Neurochem.* **1984**, 42, 1-  
672 11.

- 673 (13) Hirai, K., et al., Inhibiting neuronal migration by blocking NMDA receptors in the  
674 embryonic rat cerebral cortex: a tissue culture study. *Brain Res. Dev. Brain Res.* **1999**, 114, 63-  
675 67.
- 676 (14) Palazzo, E., Marabese, I., de Novellis, V., Rossi, F., Maione, S. Supraspinal metabotropic  
677 glutamate receptors: a target for pain relief and beyond. *Eur J Neurosci.* **2014**, 39, 444-54
- 678 (15) Li, Y., et al., Graphene microsheets enter cells through spontaneous membrane penetration  
679 at edge asperities and corner sites. *Proc Natl Acad Sci U S A* **2013**, 110, 12295-300
- 680 (16) Mao, J., Guo, R., Yan, L. T. Simulation and analysis of cellular internalization pathways  
681 and membrane perturbation for graphene nanosheets. *Biomaterials* **2014**, 35, 6069-77
- 682 (17) Rizzoli, S. O. Synaptic vesicle recycling: steps and principles. *EMBO J.* **2014**, 33, 788-822.
- 683 (18) Rodrigues, A. F., et al., A blueprint for the synthesis and characterisation of thin graphene  
684 oxide with controlled lateral dimensions for biomedicine. *2D Materials* **2018**, 5, 035020
- 685 (19) Tang, X., Ho, W. B., Xue, J. M. Synthesis of Zn-Doped AgInS<sub>2</sub> nanocrystals and their  
686 fluorescence properties. *J. Phys. Chem. C* **2012**, 116, 9769–9773.
- 687 (20) Adegoke, O., & Forbes, P. B. L-cysteine-capped core/shell/shell quantum dot-graphene  
688 oxide nanocomposite fluorescence probe for polycyclic aromatic hydrocarbon detection. *Talanta*  
689 **2016**, 146, 780-788.
- 690 (21) Shang, J., Ma, L., Li, J., Ai, W., Yu, T., Gurzadyan, G. G. The origin of fluorescence from  
691 graphene oxide. *Sci Rep.* **2012**, 2, 792
- 692 (22) Rao, M. J., Shibata, T., Chattopadhyay, S., Nag, A. Origin of photoluminescence and XAFS  
693 study of (ZnS)<sub>1-x</sub>(AgInS<sub>2</sub>)<sub>x</sub> nanocrystals. *J Phys Chem Lett.* **2014**, 5, 167-173.
- 694 (23) Li, J., Zhang, Y., Zhang, Z., Tian, Z. Facile synthesis of ZnO Nanorods/GO composite and  
695 its optical performance. *J Nanosci Nanotechnol.* **2019**, 19, 2379-2384.
- 696 (24) Vempati, S., Celebioglu, A., Uyar, T. Defect related emission versus intersystem crossing:  
697 blue emitting ZnO/graphene oxide quantum dots. *Nanoscale* **2015**, 7, 16110-16118.
- 698 (25) Raastad, M., Storm, J. F., Andersen, P. Putative single quantum and single fibre excitatory  
699 postsynaptic currents show similar amplitude range and variability in rat hippocampal slices.  
700 *Eur. J. Neurosci.* **1992**, 4, 113-117.
- 701 (26) Cellot, G., et al., Carbon nanotube scaffolds tune synaptic strength in cultured neural  
702 circuits: novel frontiers in nanomaterial-tissue interactions. *J Neurosci.* **2011**, 31, 12945-12953.
- 703 (27) Tyler, E. C., Lovinger, D. M. Metabotropic glutamate receptor modulation of synaptic

- 704 transmission in corticostriatal co-cultures: role of calcium influx. *Neuropharmacology* **1995**, 34,  
705 939-952.
- 706 (28) Malgaroli, A., Tsien, R. W. Glutamate-induced long-term potentiation of the frequency of  
707 miniature synaptic currents in cultured hippocampal neurons. *Nature* **1992**, 357, 34-39.
- 708 (29) Richter, K., et al., Gundelfinger, Presynaptic cytomatrix protein bassoon is localized at both  
709 excitatory and inhibitory synapses of rat brain. *J Comp Neurol.* **1999**, 408, 437-448.
- 710 (30) Segal, M. Rat hippocampal neurons in culture: responses to electrical and chemical stimuli.  
711 *J Neurophysiol* **1983**, 50,1249–1264.
- 712 (31) Melnick, I. V., Chvanov, M. A., Belan, P. V., Rat hippocampal neurons maintain their own  
713 GABAergic synaptic transmission in culture. *Neurosci Lett* **1999**, 262, 151–154
- 714 (32) Galante, M., Nistri, A., Ballerini, L. Opposite changes in synaptic activity of organotypic rat  
715 spinal cord cultures after chronic block of AMPA/kainate or glycine and GABAA receptors. *J*  
716 *Physiol.* **2000**, 523, 639-651.
- 717 (33) Gasparini, S., Saviane, C., Voronin, L. L., Cherubini, E. Silent synapses in the developing  
718 hippocampus: lack of functional AMPA receptors or low probability of glutamate release? *Proc*  
719 *Natl Acad Sci U S A.* **2000**, 97, 9741-9746
- 720 (34) Rozov, A., Jerecic, J., Sakmann, B., Burnashev, N. AMPA receptor channels with long-  
721 lasting desensitization in bipolar interneurons contribute to synaptic depression in a novel  
722 feedback circuit in layer 2/3 of rat neocortex. *J Neurosci.* **2001**, 21, 8062-8071
- 723 (35) Murthy, V. N., Sejnowski, T. J., Stevens, C. F. Heterogeneous release properties of  
724 visualized individual hippocampal synapses. *Neuron* **1997**, 18, 599-612
- 725 (36) Zucker, R. S. Short-term synaptic plasticity. *Annu Rev Neurosci.* **1989**, 12, 13-31.
- 726 (37) Manabe, T., Wyllie, D. J., Perkel, D. J., Nicoll, R. A. Modulation of synaptic transmission  
727 and long-term potentiation: effects on paired pulse facilitation and EPSC variance in the CA1  
728 region of the hippocampus. *J Neurophysiol.* **1993**, 70, 1451-9.
- 729 (38) Debanne, D., Guérineau, N. C., Gähwiler, B. H., Thompson, S. M. Paired-pulse facilitation  
730 and depression at unitary synapses in rat hippocampus: quantal fluctuation affects subsequent  
731 release. *J Physiol.* **1996**, 491, 163-76.
- 732 (39) Dittman, J. S., & Regehr, W. G. Calcium dependence and recovery kinetics of presynaptic  
733 depression at the climbing fiber to Purkinje cell synapse. *J Neurosci.* **1998**, 18, 6147-6162

- 734 (40) Dittman, J. S., Kreitzer, A. C., Regehr, W. G. Interplay between facilitation, depression, and  
735 residual calcium at three presynaptic terminals. *J Neurosci.* **2000**, 20, 1374-1385.
- 736 (41) Lana, D., Ugolini, F., Nosi, D., Wenk, G. L., Giovannini, M. G. Alterations in the interplay  
737 between neurons, astrocytes and microglia in the rat dentate gyrus in experimental models of  
738 neurodegeneration. *Front Aging Neurosci.* **2017**, 9, 296.
- 739 (42) Kawano, H., et al., Role of the lesion scar in the response to damage and repair of the  
740 central nervous system. *Cell Tissue Res.* **2012**, 349, 169-180
- 741 (43) Vautrin, J., & Barker, J. L. Presynaptic quantal plasticity: Katz's original hypothesis  
742 revisited. *Synapse* **2003**, 47, 184-199
- 743 (44) Kaeser, P. S., & Regehr, W. G. Molecular mechanisms for synchronous, asynchronous, and  
744 spontaneous neurotransmitter release. *Annu Rev Physiol.* **2014**, 76, 333-363
- 745 (45) Fioravante, D., & Regehr, W. G. Short-term forms of presynaptic plasticity. *Curr Opin*  
746 *Neurobiol.* **2011**, 21, 269-274
- 747 (46) Li, Y. C., Kavalali, E. T. Synaptic vesicle-recycling machinery components as potential  
748 therapeutic targets. *Pharmacol Rev.* **2017**, 69, 141-160
- 749 (47) Bramini, M., et al., Graphene oxide nanosheets disrupt lipid composition, Ca(2+)  
750 homeostasis, and synaptic transmission in primary cortical neurons. *ACS Nano* **2016**, 10, 7154-  
751 7171
- 752 (48) Sara, Y., Virmani, T., Deák, F., Liu, X., Kavalali, E. T. An isolated pool of vesicles recycles  
753 at rest and drives spontaneous neurotransmission. *Neuron* **2005**, 45, 563-573
- 754 (49) Capogna, M. Presynaptic facilitation of synaptic transmission in the hippocampus.  
755 *Pharmacol Ther.* **1998**, 77, 203-223
- 756 (50) Rosenmund, C., & Stevens, C. F. Definition of the readily releasable pool of vesicles at  
757 hippocampal synapses. *Neuron* **1996**, 16, 1197-1207
- 758 (51) High, B., Cole, A. A., Chen, X., Reese, T. S. Electron microscopic tomography reveals  
759 discrete transleft elements at excitatory and inhibitory synapses. *Front Synaptic Neurosci.* **2015**,  
760 7, 9
- 761 (52) Sun, C., et al., Graphene oxide nanosheets stimulate ruffling and shedding of mammalian  
762 cell plasma membranes. *Chem.* **2016**, 1, 273-286
- 763 (53) Dante, S., et al., Selective targeting of neurons with inorganic nanoparticles: revealing the  
764 crucial role of nanoparticle surface charge. *ACS Nano* **2017**, 11, 6630-6640.

- 765 (54) Zhang, B., Wei, P., Zhou, Z., Wei, T. Interactions of graphene with mammalian cells:  
766 molecular mechanisms and biomedical insights. *Adv Drug Deliv Rev.* **2016**, 105, 145-162
- 767 (55) Baldrighi, M., Trusel, M., Tonini, R., Giordani, S. Carbon nanomaterials interfacing with  
768 neurons: an in vivo perspective. *Frontiers Neurosci.* **2016**, 10, 250
- 769 (56) Zhou, K., et al., Graphene functionalized scaffolds reduce the inflammatory response and  
770 supports endogeneous neuroblast migration when implanted in the adult brain. *Plos One* **2016**,  
771 11, e0151589
- 772 (57) Zhao, F., Zhao, Y., Liu, Y., Chang, X., Chen, C., Zhao, Y. Cellular uptake, intracellular  
773 trafficking, and cytotoxicity of nanomaterials. *Small* **2011**, 7, 1322-1337.
- 774 (58) Musto, M., et al., 3D organotypic spinal cultures: exploring neuron and neuroglia responses  
775 upon prolonged exposure to graphene oxide. *Front Syst Neurosci.* **2019**, 13, 1.
- 776 (59) Liu, C. W., et al., Graphene-based anticancer nanosystem and its biosafety evaluation using  
777 a zebrafish model. *Biomacromolecules* **2013**, 14, 358-366.
- 778 (60) Sydlik, S. A., Jhunjhunwala, S., Webber, M. J., Anderson, D. G., Langer, R. In vivo  
779 compatibility of graphene oxide with differing oxidation states. *ACS Nano* **2015**, 9, 3866-3874.
- 780 (61) Mukherjee, S. P., et al., Detection of endotoxin contamination of graphene based materials  
781 using the TNF- $\alpha$  expression test and guidelines for endotoxin-free graphene oxide production.  
782 *PLoS One* **2016**, 11, e0166816
- 783 (62) Bosi, S., et al., From 2D to 3D: novel nanostructured scaffolds to investigate signalling in  
784 reconstructed neuronal networks. *Sci Rep.* **2015**, 5, 9562
- 785 (63) Griguoli, M., Scuri, R., Ragozzino, D., Cherubini, E. Activation of nicotinic acetylcholine  
786 receptors enhances a slow calcium-dependent potassium conductance and reduces the firing of  
787 stratum oriens interneurons. *Eur J Neurosci.* **2009**, 30, 1011-1022
- 788 (64) Cellot, G., et al., Premature changes in neuronal excitability account for hippocampal  
789 network impairment and autistic-like behavior in neonatal BTBR T+tf/j mice. *Sci Rep.* **2017**, 7,  
790 39726
- 791 (65) Tsenov, G., Mátéffyová, A., Mareš, P., Otáhal, J., Kubová, H. Intrahippocampal injection of  
792 endothelin-1: a new model of ischemia-induced seizures in immature rats. *Epilepsia* **2007**, 48, 7-  
793 13